*Manuscript
Click here to view linked References

The Formation of Laurentia: Evidence From Shear Wave Splitting

Mitch V. Liddell[1*], Ian Bastow[1], Fiona Darbyshire[2], Amy Gilligan[3],

Steven Pugh[1]

(4^{th} September 2017)

[1]Imperial College London
[2]Université du Québec à Montréal
[3]University of Aberdeen
Email: m.liddell14@imperial.ac.uk*

1 Abstract

The northern Hudson Bay region in Canada comprises several Archean cratonic nuclei, assembled by a number of Paleoproterozoic orogenies including the Trans-Hudson Orogen (THO) and the Rinkian-Nagssugtoqidian Orogen. Recent debate has focused on the extent to which these orogens have modern analogues such as the Himalayan-Karakoram-Tibet Orogen. Further, the structure of the lithospheric mantle beneath the Hudson Strait and southern Baffin Island is potentially indicative of Paleoproterozoic underthrusting of the Superior plate beneath the Churchill collage. Also in question is whether the Laurentian cratonic root is stratified, with a fast, depleted, Archean core underlain by a slower, younger, thermally-accreted layer. Plate-scale

process that create structures such as these are expected to manifest as measurable fossil seismic anisotropic fabrics. We investigate these problems via shear wave splitting, and present the most comprehensive study to date of mantle seismic anisotropy in northern Laurentia. Strong evidence is presented for multiple layers of anisotropy beneath Archean zones, consistent with the episodic development model of stratified cratonic keels. We also show that southern Baffin Island is underlain by dipping anisotropic fabric, where underthrusting of the Superior plate beneath the Churchill has previously been interpreted. This provides direct evidence of subduction-related deformation at 1.8 Ga, implying that the THO developed with modern plate-tectonic style interactions.

Keywords: Lithosphere, SKS, shear wave splitting, Hudson Bay, Precambrian tectonics, anisotropic modelling, Trans-Hudson Orogen, Nagssugtoqidian Orogen, cratons, seismic anisotropy, Laurentia.

2 Overview

The geological record of the northern Hudson Bay region in Canada exceeds 2 billion years, including several Archean nuclei and a series of Paleoproterozoic orogens that culminated in the assembly of the cratonic core of North America, Laurentia. The largest of these is the Trans-Hudson Orogen (THO), which marks the ∼1.8 Ga collision between the Archean Superior craton and the Churchill plate (Figure 1; Hoffman, 1988). Structural and thermobarometric studies suggest the THO was similar in scale and style to the modern-day Himalayan-Karakoram-Tibet Orogen (HKTO) (e.g., St-

Onge et al., 2006), a finding corroborated by seismic studies of the crust (Thompson et al., 2010; Pawlak et al., 2011; Gilligan et al., 2016a), and recently by the discovery of low-temperature, high-pressure eclogite rocks within the THO indicative of plate-scale subduction (Weller and St-Onge, 2017). Farther north are the remnants of the 1.7 Ga Nagssugtoqidian Orogen (NO; Figure 1) which records the collision of the North Atlantic, Superior, and Rae cratons with plate-scale deformation distinct from that imparted from the nearly contemporaneous THO to the south. Laurentia is also characterised by one of the deepest lithospheric roots ('keels') on Earth, with the lithospheric mantle reaching depths >280 km in places (e.g., Bao and Eaton, 2015; Porritt et al., 2015). Recent debate has centred on whether the root is stratified, with a seismically fast, depleted, upper layer underlain by a younger, slower, thermal lithosphere (e.g., Yuan and Romanowicz, 2010), and whether such a layer is restricted to Archean domains or extends beneath Proterozoic regions as well (e.g., Darbyshire et al., 2013).

Increasing our knowledge of the seismic structure of the Hudson Bay region is central to our understanding of the assembly of Laurentia. Modern-style plate tectonics would have imparted measurable, plate-scale, seismically-anisotropic fossil fabrics in the lithosphere. For example, plate-scale underthrusting of the Superior lithosphere beneath the Churchill plate could be expected to create dipping anisotropic layers with fast directions perpendicular to the direction of collision, while keel stratification should result in multiple layers of anisotropy (e.g., Yuan and Romanowicz, 2010;

Darbyshire et al., 2013).

When a radially-polarised shear wave encounters seismically anisotropic media, it will split into two orthogonal shear waves polarised along the fast and slow axes of the material. The splitting parameters ϕ (the polarisation direction of the fast shear wave) and δt (the delay time between the two waves) can then be used to characterise the crust and mantle anisotropy beneath the receiver (Silver and Chan, 1991).

Here we present the results of a shear wave splitting study of SKS and SKKS (hereafter referred to as SKS) phases recorded by 43 seismograph stations in the northern Hudson Bay region. Regional SKS splitting studies often utilise only 1-2 years of data, limiting the backazimuthal coverage of high-quality measurements, and precluding the possibility of interpreting more complicated dipping or multi-layer structures. However, our data set comprises stations with recording times between 4 and 23 years. The Hudson Bay Lithospheric Experiment (HuBLE; e.g., Bastow et al., 2011) stations in the Hudson Strait and on Baffin Island were active from 2007 to 2011. The Portable Observatories for Lithospheric Analysis and Research Investigating Seismicity (POLARIS; Eaton et al., 2005) network began deployment in 2004 in western Hudson Bay and northern Quebec. Stations FCC and FRB from the Canadian National Seismograph Network have been active since 1994.

3 Tectonic Background

Our study region contains large portions of 3 Archean provinces (Rae, Hearne, Superior: Figure 1) that comprise much of the Canadian Shield (Hoffman, 1988). The nuclei of these Archean regions are thought to have originally grown by lateral accretion and wedging of proto-continents in a pre-subduction setting (Snyder et al., 2016). The Rae and Hearne are divided by the Snowbird Tectonic Zone (STZ), potentially a 1.9 Ga collision zone (Berman et al., 2007), and together comprise the bulk of the Churchill plate. The Churchill-Superior collision is thought to have been complex, trapping several smaller micro-plates between the principal cratons before terminal collision at 1.8 Ga (Corrigan et al., 2009). Southern Baffin Island has been postulated to be an amalgamation of some of these micro-continents, including the Meta-Incognita (MI) block, the Sugluk block, and the Hall Peninsula block, together dubbed the 'MISH' block (Snyder et al., 2013). The Baffin Suture (St-Onge et al., 2006) marks the boundary between the southeast Rae craton and the Meta-Incognita (MI) microcontinent that makes up much of southern Baffin Island. The northward trending features and relatively shallow burial depth of the region indicate that Meta-Incognita was the upper plate in the Rae-MI collision (Corrigan et al., 2009).

Northern Baffin Island includes the western extension of Greenland's Paleoproterozoic Rinkian fold belt along the SE-NW oriented Northeast Baffin Thrust Belt (NBTB; Figure 1), which exerted southwesterly pressure and strikes roughly perpendicular to the structural deformation patterns to the south, overprinting several Archean and

Paleoproterozoic provinces (Jackson and Berman, 2000). This generally north-south striking fold belt has been linked to the east-west oriented plate-scale Nagssugtoqidian Orogen (NO) of southern Greenland (e.g., Connelly et al., 2006). The combined Rinkian-Nagssugtoqidian orogen is similarly asymmetric, and potentially similar in scale, to the THO to the south.

4 SKS Splitting with Cluster Analysis

Seismic anisotropy refers to the directional dependence of seismic wavespeed. When a shear wave encounters an anisotropic medium, it will split into two shear waves, orthogonally polarised, one travelling faster than the other (e.g., Silver and Chan, 1991). The polarisation direction (ϕ) of the fast shear wave, and the delay time (δt) between them can be used to characterise the seismic anisotropy of the material. P-to-S converted phases such as SKS and SKKS, are ideally-suited for upper-mantle shear-wave splitting studies; they are radially polarised at the core-mantle boundary and thus record no source-side anisotropy (e.g. Silver and Chan, 1991; Long and Silver, 2009). Olivine, the most common mineral in Earth's upper mantle, is highly anisotropic. A crystallographic preferred orientation (CPO) may develop in the olivine in response to strain, with its a-axis aligned parallel to the direction of flow (e.g. Bystricky et al., 2000; Tommasi et al., 2000; Zhang and Karato, 1995), assuming steady-state, one dimensional shear flow (Kaminski and Ribe, 2002). The shear wave splitting parameters, ϕ and δt, can therefore be related to pre-existing 'fossil' anisotropy in the lithosphere (e.g. Silver and Chan, 1991; Vauchez and Nicolas, 1991), mantle convec-

tion patterns (e.g, Vinnik et al., 1989), absolute plate motion directions (e.g, Debayle and Ricard, 2013), aligned melt/fluid (e.g., Blackman and Kendall, 1997), or any combination thereof.

We inspected SKS phases for earthquakes of mb$\geq$6 occurring at epicentral distances of $\geq$88° from 2004 to 2017. For permanent stations FRB and FCC, our search extended back to 1993. In total 5483 event-station pairs were processed, and 406 were included in the final dataset. Data were filtered prior to analysis using a zero-phase Butterworth bandpass filter with corner frequencies 0.04 and 0.3 Hz. Splitting parameters were constrained using the semi-automated approach of Teanby et al. (2004), built on the Silver and Chan (1991) method. Horizontal components are rotated and time-shifted to minimise the second eigenvalue of the covariance matrix for particle motion within a time window around the shear wave arrival. This is equivalent to linearising the particle motion and minimising tangential component shear wave energy. If the particle motion is linearised initially this is called a 'null' measurement and indicates that the anisotropic fast direction is either perpendicular or parallel to the backazimuth of the wave, or that no anisotropic material was encountered. Null measurements therefore have an inherent 90° ambiguity, and are reported in Figure 1 as a red cross. The Silver and Chan (1991) approach takes a single, manually picked, shear-wave analysis window. In the cluster analysis approach of Teanby et al. (2004), however, the splitting analysis is performed for a range of window lengths and cluster analysis is utilised to find measurements that are stable over many different windows.

All splitting parameters were determined after analysis of 100 different windows. An example of the analysis is shown in Figure 2.

5 SKS Splitting Results

The results obtained for SKS splitting in northern Canada displayed visually in Figure 1 are summarised in Table 1; a full list of all splitting results and associated errors is included in supplemental materials. The average signal to noise ratio (as defined by Restivo and Helffrich, 1999) for these data is 15.5 with a standard deviation of 7.1. Quality control was enforced by visual inspection of each split to ensure linearisation of the particle motion. We also enforced data error upper limits of $\pm 15^\circ$ in ϕ and ± 0.5 s in δt, although most were much lower (see supplemental materials for complete dataset). This is a much stricter limit than the previous study of Snyder et al. (2013), where errors sometimes exceeded $\pm 30^\circ$ in ϕ and 2s in δt. Where relevant, a model class is assigned to each stations to describes the first order type of anisotropy observed at that station (Table 1). Each basic class of model (single layer, two-layer, dipping layer) has a distinctive backazimuthal pattern in their splitting parameters. A dipping anisotropic layer will vary relatively smoothly with 360° periodicity. An anisotropic model of a vertical interface has 180° backazimuthal periodicity, and a two-layer model has 90° periodicity (Figure 3; Silver and Savage, 1994). A dipping model has peak-to-peak ϕ variations $\leq 90^\circ$, as opposed to interfaces or two-layer models, which have sharper changes in ϕ and peak-to-peak variations approaching 180°.

The model-class for each station in Table 1 is chosen to be the simplest possible that explains the observations. For many of the stations in Figure 1 a single, horizontal anisotropic layer could adequately explain the data. Data from such stations were stacked using a procedure based on the method of Wolfe and Silver (1998) to obtain single pairs of splitting parameters (e.g., CTSN, DORN, MARN, in Figure 1; Table 1). We cannot, however, preclude the possibility that this assumption is invalid for stations where backazimuthal coverage of earthquakes is insufficient to resolve more complex dipping or multi-layer patterns of anisotropy (e.g., Silver and Savage, 1994). Plots of ϕ vs backazimuth for each station in Figure 1 are in the supplemental materials. For stations that exhibited clear variation typical of a more complex anisotropic structure, a grid search of relevant model parameters was performed to forward model the ϕ and δt using the MSAT toolkit of Walker and Wookey (2012), which is capable of modelling both multi-layer and dipping anisotropy. Bastow et al. (2011) suggested the presence of dipping anisotropy based on backazimuthal variation of splitting parameters; we are the first to explore this hypothesis quantitatively. The 'N' column in Table 1 compares the number of splits used to define each station in our dataset directly to that of Bastow et al. (2011), in brackets.

Station	ϕ	δt	N	Station	ϕ	δt	N
AKVQ	84 ± 4	0.9 ± 0.1	3	MANN	82 ± 1	0.8 ± 0.1	8 (2)
AP3N	43 ± 2	0.6 ± 0.1	10	MARN	-58 ± 1	1.1 ± 0.1	16
B1NU	47 ± 8	0.5 ± 0.1	3	MNGN	-88 ± 1	1.1 ± 0.1	23 (11)
CDKN	-47 ± 5	0.7 ± 0.1	4 (2)	MUMO	73 ± 1	1.3 ± 0.1	14
CHIN	-49 ± 3	1.6 ± 0.1	3	NOTN	90 ± 1	1.6 ± 0.1	8 (6)
CLRN	86 ± 5	1.3 ± 0.1	1	NUNN	84 ± 3	0.9 ± 0.1	3 (1)
CMBN	-20 ± 1	1.3 ± 0.2	2 (2)	PINU	-86 ± 2	0.8 ± 0.1	4
CTSN	63 ± 1	0.8 ± 0.1	13 (2)	PNGN	-71 ± 2	0.7 ± 0.1	6 (2)
DORN	-85 ± 3	1.1 ± 0.1	4 (3)	QILN	67 ± 1	1.2 ± 0.1	6 (2)
INUQ	71 ± 2	0.6 ± 0.1	5	SEDN	70 ± 1	0.8 ± 0.1	10
IVKQ	-80 ± 2	0.8 ± 0.1	2	SHMN	-77 ± 3	0.7 ± 0.1	5 (2)
JENN	69 ± 14	0.7 ± 0.2	1	SILO	62 ± 1	0.6 ± 0.1	7
JOSN	59 ± 5	1.0 ± 0.1	2	SMLN	14 ± 4	0.6 ± 0.1	2
KASO	91 ± 2	1.1 ± 0.1	4	SRLN	44 ± 1	0.7 ± 0.1	5
KAJQ	-71 ± 8	0.3 ± 0.1	2	STLN	-9 ± 2	1.0 ± 0.1	3
KIMN	-76 ± 2	0.7 ± 0.1	6 (3)	VIMO	83 ± 1	0.6 ± 0.1	9
KJKQ	51 ± 2	0.7 ± 0.1	7	WAGN	54 ± 1	1.5 ± 0.1	8 (2)
KNGQ	-58 ± 2	1.1 ± 0.1	5	YBKN	-27 ± 5.25	0.3 ± 0.1	4
LAIN	56 ± 2	1.0 ± 0.1	7				

Station	ϕ	δt	N	Station	ϕ	δt	N
Multiple				$ILON_{300-360}$	140 ± 5	1.1 ± 0.2	1
$ARVN_{0-90}$	46 ± 4	1.1 ± 0.09	1	$ILON_{2}$	null	-	2
$ARVN_{90-180}$	29 ± 5	1.5 ± 0.10	1	$ILON_{290}$	null	-	3
$ARVN_{180-275}$	45 ± 2	0.8 ± 0.02	7	$ILON_{316}$	null	-	-
$ARVN_{275-300}$	61 ± 5	0.9 ± 0.04	1	$ILON_{327}$	null	-	-
$ARVN_{300-315}$	-89 ± 9	0.7 ± 0.06	1	$ILON_{330}$	null	-	2
$ARVN_{315-360}$	59 ± 4	1.5 ± 0.09	2	$ILON_{334}$	null	-	3
$ARVN_{320}$	null	-	2	$SHWN_{90-180}$	0 ± 4	1.4 ± 0.1	1
$BULN_{90-275}$	56 ± 6	1.0 ± 0.10	5 (2)	$SHWN_{180-360}$	128 ± 9	0.5 ± 0.1	1
$BULN_{275-360}$	114 ± 7	0.9 ± 0.20	6 (-)	$SHWN_{282}$	null	-	-
FCC_{0-90}	55 ± 4	0.9 ± 0.1	2	$SHWN_{259}$	null	-	-
FCC_{90-180}	2 ± 10	0.7 ± 0.1	2	**Dipping**			
$FCC_{180-275}$	41 ± 1	0.8 ± 0.1	29	FRB_{0-90}	126 ± 2	1.1 ± 0.1	3 (-)
$FCC_{275-300}$	77 ± 6	0.6 ± 0.1	2	FRB_{90-183}	52 ± 8	0.6 ± 0.1	3 (1)
$FCC_{300-315}$	90 ± 4	0.9 ± 0.1	5	$FRB_{183-270}$	62 ± 7	0.9 ± 0.1	3 (2)
$FCC_{315-360}$	41 ± 1	0.8 ± 0.1	6	$FRB_{270-300}$	83 ± 1	0.9 ± 0.1	19 (10)
FCC_{316}	null	-	-	$FRB_{300-330}$	103 ± 2	0.7 ± 0.1	9 (6)
FCC_{320}	null	-	3	$FRB_{330-360}$	107 ± 4	0.7 ± 0.1	5 (1)
FCC_{325}	null	-	3	HP_{0-90}	123 ± 1	1.3 ± 0.1	5
FCC_{327}	null	-	-	HP_{90-180}	70 ± 18	0.6 ± 0.2	3
Interface				$HP_{180-270}$	77 ± 4	0.9 ± 0.1	3
$CRLN_{110-180}$	5 ± 7	1.2 ± 0.20	1 (2)	$HP_{270-300}$	84 ± 1	0.9 ± 0.1	21
$CRLN_{300-360}$	97 ± 11	0.8 ± 0.50	9 (1)	$HP_{300-330}$	99 ± 2	0.8 ± 0.1	18
$GIFN_{90-180}$	7 ± 5	1.3 ± 0.2	4	$HP_{330-360}$	102 ± 2	0.8 ± 0.1	19
$GIFN_{180-360}$	140 ± 4	0.7 ± 0.1	1	**Null Only**			
$GIFN_{269}$	null	-	-	$KUGN_{258}$	null	-	2
$ILON_{90-180}$	30 ± 2	0.8 ± 0.1	8	$KUGN_{319}$	null	-	-
$ILON_{180-300}$	106 ± 4	0.9 ± 0.1	3	$KRSQ_{346}$	null		

Table 1: SKS Splitting parameters for stacked (top) and unstacked (bottom) stations. Subscript values refer to backazimuth ranges for binned results, or the backazimuth of recording for null measurements. N is the number of splits (including nulls) for that station or backazimuthal range, bracketed numbers are the number of splits used by Bastow et al. (2011) for the same station. For unstacked results, bold type text indicates the first-order model class groups based on Figure 3.

176

177 6 Discussion

178 6.1 Causes of Observed Anisotropy

179 Across our study area, we commonly observe $\delta t \geq 1$ s (Figure 1, Table 1), implying
180 a mantle contribution to the observations: regional continental crust is ∼40 km thick
181 and can only reasonably account for $\delta t \leq 0.5$ s (Barruol and Mainprice, 1993; Silver,
182 1996). North American absolute plate motion (APM) is ∼22 mm/yr, well below
183 the ∼40 mm/yr sometimes considered a minimum for basal drag fabric development
184 (e.g., Debayle and Ricard, 2013; Martin-Short et al., 2015). We observe no consistent,
185 network-wide alignment with the current APM direction, which has been relatively
186 constant for the past ∼50 Myr (Müller et al., 2016). Although we cannot preclude
187 the possibility that older basal drag fabrics exist beneath the region, asthenospheric
188 fabrics due to APM or regional mantle flow (e.g., Forte et al., 2015) would, according
189 to Fresnel Zone arguments (Alsina and Snieder, 1995), be expected to produce only
190 gradual variations in ϕ and δt across our network. Our observed splitting parameters,
191 in fact, vary over horizontal length-scales as

192 as ∼150 km (e.g., Southampton Island stations versus CTSN, Figure 6). We therefore
193 reject APM as an interpretation for our observed anisotropy, as opposed to Snyder
194 et al. (2013) who interpreted APM as contributing a lower layer of anisotropy across

the entirety of the Hudson Bay region. The paucity of tectonic activity since ∼1.8 Ga rules out aligned melt as a plausible cause of the observed anisotropy, so our discussion proceeds on the assumption that our data are primarily sensitive to fossil lithospheric anisotropy, consistent with earlier studies of the region (Bastow et al., 2011).

Several stations in Table 1 exhibit strong backazimuthal variation in splitting parameters, implying the presence of complex structure, including multiple and/or dipping anisotropic layers. We address these issues in the following sections on a region-by-region basis.

6.2 Evidence for Proterozoic Plate-Scale Underthrusting Beneath Baffin Island

Fast directions for stations in the Hudson Strait and along the northern coast of Quebec and southern coast of Baffin Island tend to parallel the strike of the THO (Figure 1; Stations AKVQ, MANN, CTSN, IVKQ, NOTN, DORN, CHIN, KIMN, KNGQ). This interpretation is supported by the general trend in anisotropic direction found by Darbyshire et al. (2013) using surface waves, and the earlier SKS splitting study of Bastow et al. (2011). Unfortunately, the easternmost stations, KRSQ and KAJQ, had very few successful splits and so cannot be used to confirm or refute the THO hypothesis. Lithospheric-scale THO deformation clearly exerts first-order control on the anisotropy. The approximately EW fast direction of PNGN parallels the Baffin suture to the west of the station. At CMBN, ϕ aligns more closely with the SE turn of the suture. At station PNGN, ϕ parallels the APM direction, but the short length scale change compared to station CMBN, less than 100 km away, suggests strongly that the source of the anisotropy is more likely within the ∼200 km-thick lithosphere

in this region (Alsina and Snieder, 1995; Porritt et al., 2015).

Stations FRB, CDKN, JENN, and MNGN lie within the Hall Peninsula. To first order, ϕ at MNGN and CDKN parallels the trace of the THO, but JENN is nearly perpendicular (Figure 1). The reason for this becomes clear in Figure 4; JENN records a split from a backazimuth not sampled by CDKN or MNGN, but mirrors observations at FRB at similar backazimuths (Figure 4), giving credence to the idea that these stations sample similar structure and warrant consideration as a composite 'Hall Peninsula' or 'HP' station with good backazimuthal coverage. The stations included in the 'HP' stack were chosen based on their proximity to FRB (which provides most of the data and backazimuthal coverage to the stack) and because they share similar local geology. The Hall Peninsula region (Figure 1) is characterised by high grade metamorphism, and was part of the leading edge of the Churchill plate during the THO (St-Onge et al., 2006, 2009). Nearby stations KIMN and DORN are not included in the HP group because KIMN lies on the other side of the Soper River suture from the rest of the stations, and DORN has lower grade metamorphism on the western reaches of Baffin Island. The splitting parameters for all HP stations were stacked within appropriate backazimuth bins (Table 1, Figure 5), revealing a clear, smoothly-varying 360° periodicity, without the sharp changes in ϕ that are characteristic of multi-layer anisotropy (Figure 3). Therefore, that class of model was used to initialise an MSAT modelling procedure to characterise the anisotropic structure.

A grid search varying layer dip, up-dip direction, and olivine a-axis azimuth (AAZ) orientation was performed and the root mean squared (RMS) misfit between the model response for each set of parameters and the amalgam HP station data was calculated to indicate the agreement between model and observations. RMS was

calculated using the formula: $RMS = \sqrt{\frac{1}{n}(x_1^2 + x_2^2 \ldots x_n^2)}$ where n is the number of observed data points, and x is the difference between the data point and the modelled curve, less the error. Data points were assumed to have errors in backazimuth of $\pm 5^\circ$. The best fitting model was determined by the lowest combined RMS for both for ϕ and δt. The RMS values for each splitting parameter were normalised for each cell in the grid search, then combined (Figure 5, top) such that the maximum value in each grid is 1. This method ensures that both ϕ and δt are included in the determination of the best fitting model parameters.

Figure 5 shows the results of the grid search for the three model parameters. Initially, AAZ=0° (aligned with the dip direction), the simplest possible scenario. The minimum RMS value gives an updip direction of 265°±10° and a dip angle of 70°±5°. These values are then held constant while varying the other two parameters to confirm the best fitting model values. The middle and right RMS surfaces in Figure 5 confirm that fan AAZ of 0° is appropriate. The best fitting model is therefore a layer dipping at 70°, with a dip direction of N85°E (updip direction of 265°). These parameters yield an RMS of 5.0° and 0.12 s, for ϕ and δt, respectively. Layer thickness and olivine alignment fraction had no effect on the pattern of the splitting parameters; the effect was limited to a static shift of δt, and is therefore not well defined. What can be confidently concluded is that SKS splitting resolves a significant amount of eastward dipping anisotropy beneath southern Baffin Island. Such a dipping layer is consistent with recent findings of eclogite rocks in the THO indicative of deep plate-scale subduction (Weller and St-Onge, 2017). Our HP block results therefore provide compelling support for the hypothesis that the Superior plate underthrust the Churchill plate in a modern-style plate tectonic collision at ∼1.8 Ga.

6.3 Evidence for Lithospheric Subdivisions: Implications for the Two-Plate THO Hypothesis

Splitting parameters for stations on Southampton Island (SI) are clearly distinguished from the nearby Hudson Strait stations: ϕ varies sharply between 315° and 180° backazimuth at stations CRLN, SHWN, and SHMN, while CTSN can be explained easily by a single, horizontal anisotropic layer (Figure 6). With no data points at backazimuths $\leq$180°, we cannot confidently determine the precise anisotropic model that would best explain the observations. However, we can discount some possibilities by observing that the smoothly varying ϕ over 180° backazimuth (Figure 6) is uncharacteristic of a two-layer model (which has a periodicity of 90°); peak-to-peak variations of ϕ ($\sim$135°) are larger than expected ($\leq$90°) for a dipping layer (Figures 3, 5). Further, the low metamorphic grade of Southampton Island rocks indicates that SI has not undergone the same deformation and uplift as the higher-grade rocks on southern Baffin Island (St-Onge et al., 2009). Superior plate underthrusting, and a dipping layer, is therefore less likely in this region.

A more plausible explanation for the Southampton Island observations could be lateral variations in anisotropy due to a nearby terrane boundary. This interpretation is in line with magnetotelluric evidence of a thickening resistive crust to the northeast of Southampton Island, which was interpreted as a potential terrane boundary by Spratt et al. (2012). Such a boundary could potentially be an extension of the Rae-Hearne boundary (Snowbird Tectonic Zone: Figure 1), or an extension of the MISH block beneath this region. Similar Vp/Vs ratios and metasedimentary rocks between SI and mainland Rae (Thompson et al., 2010) support the former, while geological models by Corrigan et al. (2009) support the latter.

While the nature of the boundary cannot be confirmed from our data, the extension of the STZ onto Southampton Island is less likely than an influence from the MISH block because of the similarity in ϕ between the Rae and the Hearne on the mainland (Figure 1). Stations NUNN, WAGN, and QILN on the Rae mainland, and SEDN and JOSN on the Hearne (Figure 1), parallel THO-related deformation rather than the SI pattern shown in Figure 6. Therefore, Southampton Island is anisotropically distinct both from the cratonic provinces (Rae/Hearne) to the north and the Hudson Strait to the south. This strongly suggests that Southampton Island is part of a lithospheric block separate from the Superior or the Churchill plates. Our observations in this region thus imply that the THO cannot be considered as a simple two-plate Proterozoic collision.

6.4 Northerly Extent of the THO on Melville Peninsula

The north-central Rae domain is dominated by granite-greenstone rocks with Paleoproterozoic deformation zones, potentially having been reworked by far-field THO pressure (Carson et al., 2004). With the notable exception of station BULN, the stations on the central Rae craton in Figure 1 parallel these surface structural trends. The average anisotropic fast direction for the Melville Peninsula stations LAIN, AP3N, and SRLN, is 34°, the same orientation found for mantle-depth geoelectric strike by Spratt et al. (2013) (Figure 7). Studies by Berman et al. (2005) and Corrigan et al. (2009) also noted strong NE-SW geological trends in this regions, and related them to late-Archean events followed by THO related deformation. Stations MARN and PINU on northern Baffin Island display ϕ values that parallel the Northeast Baffin Thrust Belt (Jackson and Berman, 2000), which is the western extent of the Nagssugtoqidian orogen (NO) preserved in modern-day Greenland.

ILON and GIFN (Figure 8) have strongly varying fast direction, however, we do not present any modelling of these stations because of the lack of reliable results from the 0-180° backazimuth. The peak-to-peak variation of ϕ for ILON/GIFN in Figure 8 precludes the possibility of a dipping layer, and the data are not 90° periodic as expected for two-layer systems (Figure 3). Although we cannot preclude the possibility that multi-layer anisotropy exists here, our data coverage limits us to discussion of the variable ϕ, and comparison with nearby, less variable, stations. Stations GIFN and ILON lie between the two orogen-dominated regions and display variable ϕ values that show influence from both (Figure 8). At southerly backazimuths, ϕ values are close to those observed on the mainland of Melville Peninsula, but significantly change to parallel the Baffin Island stations as backazimuth increases to $\sim$300° (Figure 8). These stations represent a transect through deformation regimes, and therefore mark the approximate limit of Proterozoic deformation both from the south and the north. It is expected that orogenies of the size of the THO and the NO will will overprint any previous anisotropic signature. This is consistent with the view that fossil lithospheric anisotropy documents the last major tectonic event in a region (Silver and Chan, 1991). This has been previously interpreted for Melville Peninsula near ILON and GIFN (Spratt et al., 2013; Berman et al., 2005). Our results indicate a THO-related deformation zone $\sim$700 km wide, similar to the width of $\geq$650 km suggested by Gilligan et al. (2016a) across the northern Quebec-southern Baffin transect, and comparable to the 400 – 1000 km width of the modern-day Tibetan plateau.

6.5 Implications for 2-stage Keel Formation

Western Hudson Bay stations FCC and ARVN have wide backazimuthal coverage and similar variations in ϕ and δt (Figure 9). For both stations ϕ varies from $\sim$45° to $\sim$20° but increases sharply around 270° backazimuth to $\sim$90°. This pattern most closely resembles the 90° periodicity of the 2-layer synthetic model in Figure 3. Station BULN has a similar, but less clear, pattern of splitting parameters. It potentially warrants discussion as a multi-layer model also, but a relatively simple 2-layer system is not capable of recreating the observations. The cratonic nucleus of the Rae province grew by accreting terranes to its boundaries (Snyder et al., 2016). The variability of ϕ observed at BULN, which lies on one of these accreted terranes, could be from complex anisotropic fabrics that are the remains of these Archean-age accretionary processes, but nearby stations lack the backazimuthal coverage to corroborate this interpretation.

Snyder et al. (2013) published receiver function results and anisotropic ϕ values for a two-layer system for station FCC (Table 2 and Figure 8 of Snyder et al., 2013). We used the receiver functions to define potential layer thicknesses for their ϕ values and created a model with which to compare our data. This model has a ϕ of 31° overlying 79°, with layer depths of 50 km and 130 km and is plotted as the solid line in Figure 9. The model periodicity qualitatively fits our data and supports the interpretation of 2-layer anisotropy in this region. At backazimuths of $\sim$315°, however, the data are less well matched, indicating that the model may be too simplistic. More recently published results from Darbyshire et al. (2013) show that the lithosphere-asthenosphere boundary in this region is at $\sim$240 km depth; a value much deeper than the lower anisotropic layer used to produce the model in Figure 9. Further, the similarity between the FCC and ARVN data in Figure 9 links the structure beneath

these stations, thus precluding the Lynn Lake fault (local to station FCC) from being the upper layer of anisotropy. A layered lithosphere model resulting from episodic cratonic development thus fits the observations better than one requiring APM.

Cratonic regions are typically underlain with exceptionally thick (∼250 km) high wavespeed lithospheric keels. The highly-depleted cratonic core obtains a thermally accreted, more fertile boundary layer at some point after initial cratonic development, probably no earlier than the Paleoproterozoic (Yuan and Romanowicz, 2010; Bastow et al., 2013; Bao et al., 2016; Boyce et al., 2016). Support for this interpretation comes from studies such as Yuan et al. (2011) and Darbyshire et al. (2013), which have found evidence for a stratified lithosphere, cratonic and otherwise, in North America using SKS splitting, long-period seismic wave inversion, and surface wave tomography. A variety of receiver function and SKS splitting studies have also suggested the presence of a sharp change in seismic velocity at mid-lithospheric depths in North America (e.g., Miller and Eaton, 2010; Yuan and Romanowicz, 2010). While our results do not support a simple two-layer model for this region, they are consistent with the presence of multiple layers exhibiting complex anisotropy and are therefore consistent with the presence of an MLD predicted by the two-stage cratonic development theory.

7 Conclusions

We have investigated seismic anisotropy across much of the northern Hudson Bay and Baffin Island region of Canada using shear-wave splitting analysis of up to 23 years of SKS and SKKS phases. Below the Archean western coast of Hudson Bay we find strong evidence for at least two anisotropic layers in the lithosphere. Our observations are interpreted to be due to cratonic stratification and support a multi-stage

keel development theory (e.g., Yuan and Romanowicz, 2010). More broadly across the study area, however, we observe a prevalence of anisotropic fast polarisation directions that parallel the strike of the Paleoproterozoic Trans Hudson Orogen (THO), implying that it imparted plate-scale anisotropic fabrics on the region at ∼1.8 Ga. Variations in ϕ on Southampton Island reveal a unique mantle anisotropy signature consistent with the presence of a micro-continent (Meta-Incognita) caught between the colliding Churchill and Superior plates. This points to a more complex model than a simple two-plate system for the THO. The periodicity of ϕ and δt for stations on southern Baffin Island indicates the presence of dipping anisotropy. We interpret the anisotropy to be due to the Superior plate underthrusting the Churchill at ∼1.8 Ga. THO-parallel plate-scale anisotropic fabrics persist as far north as Melville Peninsula, implying THO deformation was as laterally extensive (∼700 km) as in the Himalayas today. Our results thus constitute strong evidence that modern-style plate tectonics were in action during, and were responsible for, Paleoproterozoic orogens.

8 Acknowledgments

The authors would like to thank A. Walker for invaluable help understanding the MSAT forward modelling code, as well as A. Boyce, L. Petrescu, and C. Ogden of the ICcratons group for numerous enlightening conversations about Canadian Precambrian geology and beyond. M.V. Liddell is funded by an Imperial College President's Scholarship. F.A. Darbyshire is supported by the Natural Sciences and Environment Research Council of Canada through their Discovery Grant and Canada Research Chair programmes.

9 Table and Figure Captions

Table 1. SKS Splitting Parameters for Stacked (top) and Unstacked (bottom) Stations. Subscript values refer to backazimuth ranges for binned results, or the backazimuth of recording for null measurement. N, number of splits used in stack; Class, first-order model class based on Figure 3.

Figure 1. Geological map of northern Hudson Bay with SKS splitting results. Dashed yellow bars indicate stacked ϕ and δt values, solid yellow bars indicate unstacked individual measurements. Red bars are null measurements with 90° ambiguity. Absolute plate motion arrows are purple. The inset global map shows the location of the receiver network, the red dots are earthquakes used in this study. BaS, Baffin Suture; CI, Coats Island; HP, Hall Peninsula; MI, Meta-Incognita; SI, Southampton Island; SRS, Soper River Suture; STZ, Snowbird Tectonic Zone; THO, Trans-Hudson Orogen; NBTB, Northeast Baffin Thrust Belt; NO, Nagssugtoqidian Orogen; LL, Lynn Lake Fault; MISH, Meta-Incognita-Sugluk-Hall-Peninsula.

Figure 2. High-quality splitting measurement example from station ILON. (a) The recorded seismogram showing the SKS phase and the initial window. (b) The seismogram rotated into radial and tangential components both before (top two) and after (bottom two) processing. (c) top L-R: close up of the SKS phases for the fast and slow waveforms before correction, after correction, and after correction without normalised amplitudes. Bottom L-R: particle motion before and after correction. (d) Contour map showing stability of the splitting parameters. Lines indicate one standard deviation. The thick line indicates 95 per cent confidence. (e) Splitting parameter variations as a function of the changing window. (f) Cluster analysis results for ϕ and δt for each of the 100 windows. These values were very stable over the full

range of windows.

Figure 3. MSAT calculated ϕ responses for three basic classes of anisotropy. $\Delta\phi$ indicates difference in fast direction between layers. Layer thickness and alignment fraction of olivine a-axis does not affect the patterns.

Figure 4. Splitting parameters for HP block stations on southern Baffin Island (Figure 1). Null measurements are indicated by dashed lines with diamonds at the parallel/perpendicular to backazimuth points.

Figure 5. (Top) Normalised RMS misfit surfaces for ϕ and δt combined. Left surface sets olivine a-axis to 0° relative to dip direction. The parameters with lowest RMS misfit are each kept constant individually in the next two surfaces. (Below) Modelled response for the best fitting dip, a-axis orientation, and up-dip direction plotted against stacked HP block splitting parameters.

Figure 6. Splitting parameters for the stacked Southampton Island stations and nearby CTSN, in Hudson Strait. Both groups are stacked in backazimuth bins: 0-90°, 90-180°,180-285°, 285-330°, and 330-360°. Solid black line is the best fitting HP model from Figure 5.

Figure 7. Geological map of Melville Peninsula and northern Baffin Island with SKS splitting results. Dashed yellow bars indicate stacked ϕ and δt values, solid yellow bars indicate unstacked individual measurements. Red crosses are null measurements with 90° ambiguity. Legend is the same as Figure 1. THO, Trans-Hudson Orogen; NBTB, Northeast Baffin Thrust Belt.

Figure 8. Fast direction as a function of backazimuth showing similarities between GIFN/ILON and two single-layer-interpreted regions at different backazimuths. Mainland Melville stations are AP3N/LAIN/SRLN. Baffin Island stations are MARN/PINU.

Figure 9. Fast direction and delay time as a function of back azimuth for both Western Hudson Bay stations. Null measurements are dashed lines with diamonds at the parallel/perpendicular to backazimuth points. The similarity is such that the same structure can be interpreted beneath each station. The black line is a 2-layer model with a 50 km thick upper layer with ϕ =31° over an 80 km thick layer with ϕ =79°.

References

Alsina, D., Snieder, R., 1995. Small-scale sublithospheric continental mantle deformation: constraints from SKS splitting observations. J. Geophys. Res., 115 (9), 1–24.

Bao, X., Eaton, D.W., 2015. Large variations in lithospheric thickness of western Laurentia: Tectonic inheritance or collisional reworking?. Precambrian Research, 266, 579-586.

Bao, X., Eaton, D.W., Gu, Y.J., 2016. Rayleigh wave azimuthally anisotropic phase velocity maps beneath western Canada. J. Geophys. Res., 121, 1821-1834.

Barruol, G., Mainprice, D., 1993. A quantitative evaluation of the contribution of crustal rocks to the shear-wave splitting of teleseismic SKS waves. Phys. Earth Planet. Int. 78 (3-4), 281–300.

Bastow, I. D., Kendall, J. M., Helffrich, G. R., Thompson, D. A., Wookey, J., Brisbourne, A. M., Hawthorn, D., Eaton, D. W., Snyder, D. B., 2011. The Hudson Bay Lithospheric Experiment. Astro. and Geophys. 52 (6), 21–24.

Bastow, I. D., Eaton, D. W., Kendall, J. M., Helffrich, G. R., Snyder, D. B., Thompson, D. A., Wookey, J., Darbyshire, F., Pawlak, A. E., 2013. The Hudson Bay Lithospheric Experiment (HuBLE): insights into Precambrian plate tectonics and the development of mantle keels. Geological Society Lond., Spec. Pubs. 389 (1), 41–67.

Berman, R. G., Davis, W., Pehrsson, S., 2007. Collisional Snowbird tectonic zone resurrected: Growth of Laurentia during the 1.9 Ga accretionary phase of the Hudsonian orogeny. Geology 35 (10), 911–914.

Berman, R. G., Sanborn-Barrie, M., Stern, R. A., Carson, C. J., 2005. Tectonometamorphism at ca. 2.35 and 1.85 Ga in the Rae domain, western Churchill province, Nunavut, Canada: insights from the structural, metamorphic and in situ geochronological analysis of the southwestern Committee Bay belt. The Canadian Mineralogist 43 (1), 409–442.

Blackman, D., Kendall, J. M., 1997. Sensitivity of teleseismic body waves to mineral texture and melt in the mantle beneath a midocean ridge. Philosoph. Trans. R. Soc. A 355, 217–231.

Boyce, A., Bastow, I. D., Darbyshire, F., Ellwood, A. G., Gilligan, A., Menke, W., 2016. Subduction Beneath Laurentia Modified the North American Craton Edge : Evidence from P and S-wave Tomography. J. Geophys. Res. 121, 5013–5030.

Bystricky, M., Kunze, K., Burlini, L., Burg, J.-P., 2000. High shear strain of olivine aggregrates: rheological and seismic consequences. Science 290, 1564–1567.

Carson, C. J., Berman, R. G., Stern, R. A., Sanborn-Barrie, M., Skulski, T., Sandeman, H. A., 2004. Age constraints on the Paleoproterozoic tectonometamorphic history of the Committee Bay region, western Churchill Province, Canada: evidence from zircon and in situ monazite SHRIMP geochronology. Can. J. Earth Sci. 41 (9), 1049–1076.

Connelly, J., Thrane, K., Krawiec, A., Garde, A., 2006. Linking the Palaeoproterozoic Nagssugtoqidian and Rinkian orogens through the Disko Bugt region of West Greenland. J. Geol. Soc. 163 (2), 319–335.

Corrigan, D., Pehrsson, S., Wodicka, N., De Kemp, E. A., 2009. The Palaeoproterozoic Trans-Hudson Orogen: a prototype of modern accretionary processes. Geol. Soc. Lond., Spec. Pubs. 327, 457–479.

528 Darbyshire, F., Eaton, D. W., Bastow, I. D., 2013. Seismic imaging of the lithosphere
529 beneath Hudson Bay: Episodic growth of the Laurentian mantle keel. Earth Planet.
530 Sci. Lett. 373, 179–193.

531 Debayle, E., Ricard, Y., 2013. Seismic observations of large-scale deformation at the
532 bottom of fast-moving plates. Earth Planet. Sci. Lett. 376, 165–177.

533 Eaton, D. W., Adams, J., Asudeh, I., Atkinson, G. M., Bostock, M. G., Cassidy, J. F.,
534 Ferguson, I. J., Samson, C., Snyder, D. B., Tiampo, K. F., Unsworth, M. J., 2005.
535 Investigating Canada's Lithosphere and earthquake hazards with portable arrays.
536 Eos, Transactions Am. Geophys. Un. 86 (17), 169.

537 Forte, A. M., Simmons, N. A., Grand, S. P., 2015. Constraints on 3-D Seismic Models
538 from Global Geodynamic Observables: Implications for the Global Mantle Convec-
539 tive Flow. In: Romanowicz, B., Dziewonski, A. M. (Eds.), Treatise on Geophys.,
540 2nd Edition. No. 1. Elsevier, Amsterdam, pp. 853–907.

541 Gilligan, A., Bastow, I. D., Darbyshire, F., 2016a. Seismological structure of the 1.8
542 Ga Trans-Hudson Orogen of North America. Geochem., Geophys., Geosyst. 17,
543 2421–2433.

544 Hoffman, P. F., 1988. United Plates of America, the birth of a craton: Early Pro-
545 terozoic assembly and growth of Laurentia. Ann. Rev. Earth Planet. Sci. 16 (1),
546 543–603.

547 Jackson, G. D., Berman, R. G., 2000. Precambrian Metamorphic and Tectonic Evo-
548 lution of Northern Baffin Island, Nunavut, Canada. The Canadian Mineralogist 38,
549 399–421.

550 Kaminski, É., Ribe, N. M., 2002. Timescales for the evolution of seismic anisotropy
551 in mantle flow. Geochem., Geophys., Geosyst. 3 (8), 1–17.

552 Long, M. D., Silver, P. G., 2009. Shear wave splitting and mantle anisotropy: Mea-
553 surements, interpretations, and new directions. Surv. Geophys. 30 (4-5), 407–461.

554 Martin-Short, R. A., Richard, M., Bastow, I. D., Totten, E., Richards, M., 2015.
555 Mantle flow geometry from ridge to trench beneath the Gorda - Juan de Fuca plate
556 system. Nature Geoscience, 8 (December), 1–21.

557 Miller, M. S., Eaton, D. W., 2010. Formation of cratonic mantle keels by arc accretion:
558 Evidence from S receiver functions. Geophys. Res. Lett. 37 (18), 1–5.

559 Müller, R. D., Seton, M., Zahirovic, S., Williams, S. E., Matthews, K. J., Wright,
560 N. M., Shephard, G. E., Maloney, K. T., Barnett-Moore, N., Bower, D. J., Can-
561 non, J. S., 2016. Ocean basin evolution and global-scale reorganization events since
562 Pangea breakup. Ann. Rev. Earth Planet. Sci. Lett. 44, 107–138.

563 Pawlak, A., Eaton, D., Bastow, I., Kendall, J.-M., Helffrich, G., Wookey, J., Snyder,
564 D., 2011. Crustal structure beneath Hudson Bay from ambient noise tomography:
565 implications for basin formation. Geophys. J. Int. 184 (1), 65–82.

566 Porritt, R. W., Miller, M. S., Darbyshire, F., 2015. Lithospheric architecture beneath
567 Hudson Bay. Geochem., Geophys., Geosyst. 16 (7), 2262–2275.

568 Restivo, A., Helffrich, G., 1999. Teleseismic shear wave splitting measurements in
569 noisy environments. Geophys. J. Int. 137 (3), 821–830.

570 Silver, P. G., 1996. Seismic anisotropy beneath the continents: Probing the Depths
571 of Geology. Ann. Rev. Earth Planet. Sci. 24 (1), 385–432.

572 Silver, P. G., Chan, W. W., 1991. Shear Wave Splitting and Subcontinental Mantle
573 Deformation. J. Geophys. Res. 96 (B10), 16429–16454.

574 Silver, P. G., Savage, M. K., 1994. The interpretation of shear-wave splitting param-
575 eters in the presence of two anisotropic layers. Geophys. J. Int. 119, 949–963.

576 Snyder, D. B., Berman, R. G., Kendall, J. M., Sanborn-Barrie, M., 2013. Seismic
577 anisotropy and mantle structure of the Rae craton, central Canada, from joint
578 interpretation of SKS splitting and receiver functions. Precambrian Res. 232, 189–
579 208.

580 Snyder, D. B., Humphreys, E., Graham Pearson, D., 2016. Construction and destruc-
581 tion of some North American cratons. Tectonophysics 694, 464–485.

582 Spratt, J. E., Craven, J. A., Sanborn-Barrie, M., 2012. Southampton Island magne-
583 totelluric survey: data acquisition and preliminary analysis. Geological Survey of
584 Canada Open File, 6988, 39p.

585 Spratt, J. E., Jones, A. G., Corrigan, D., Hogg, C., Canada, N. R., 2013. Litho-
586 spheric geometry beneath Melville Peninsula, Nunavut, revealed by deep-probing
587 magnetotelluric surveying. Geological Survey of Canada, Current Research 12, 14p.

588 St-Onge, M. R., Searle, M. P., Wodicka, N., 2006. Trans-Hudson orogen of North
589 America and Himalaya-Karakoram-Tibetan orogen of Asia: Structural and thermal
590 characteristics of the lower and upper plates. Tectonics 25 (4), 1–22.

591 St-Onge, M. R., Van Gool, J. A. M., Garde, A., Scott, D. J., 2009. Correlation of
592 Archaean and Palaeoproterozoic units between northeastern Canada and western
593 Greenland: constraining the pre-collisional upper plate accretionary history of the
594 Trans-Hudson orogen. Geol. Soc. Lond., Spec. Pubs. 318 (1), 193–235.

595 Teanby, N., Kendall, J.-M. van der Baan, M., 2004. Automation of Shear-Wave Split-
596 ting Measurements using Cluster Analysis. Bull. Seism. Soc. Am., 94 (2), 453–463.

597 Thompson, D. A., Bastow, I. D., Helffrich, G. R., Kendall, J. M., Wookey, J., Snyder,
598 D. B., Eaton, D. W., 2010. Precambrian crustal evolution: Seismic constraints from
599 the Canadian Shield. Earth Planet. Sci. Lett. 297 (3-4), 655–666.

Tommasi, A., Mainprice, D., Canoval, G., Chastel, Y., 2000. Viscoplastic self-consistent and equilibrium-based modeling of olivine lattice preferred orientations: Implications for the upper mantle seismic anisotropy. J. Geophys. Res. 105 (B4), 7893–7908.

Vauchez, A., Nicolas, A., 1991. Mountain building: strike-parallel motion and mantle anisotropy. Tectonophysics 185 (3-4), 183–201.

Vinnik, L. P., Farra, V., Romanowicz, B., 1989. Azimuthal Anisotropy in the Earth From Observations of SKS At Geoscope and NARS Broadband Stations. Bull. Seism. Soc. Am., 79 (5), 1542–1558.

Weller, O., St-Onge, M.R., 2017. MSAT- A new toolkit for the analysis of elastic and seismic anisotropy. Comput. and Geosci. 49, 81–90.

Walker, A. M., Wookey, J., 2012. Record of modern-style plate tectonics in the Palaeo-proterozoic Trans-Hudson orogen. Nature Geoscience, 10, 305–312.

Wolfe, C. J., Silver, P. G., 1998. Seismic anisotropy of oceanic upper mantle: Shear wave splitting methodologies and observations. J. Geophys. Res. 103 (B1), 749–771.

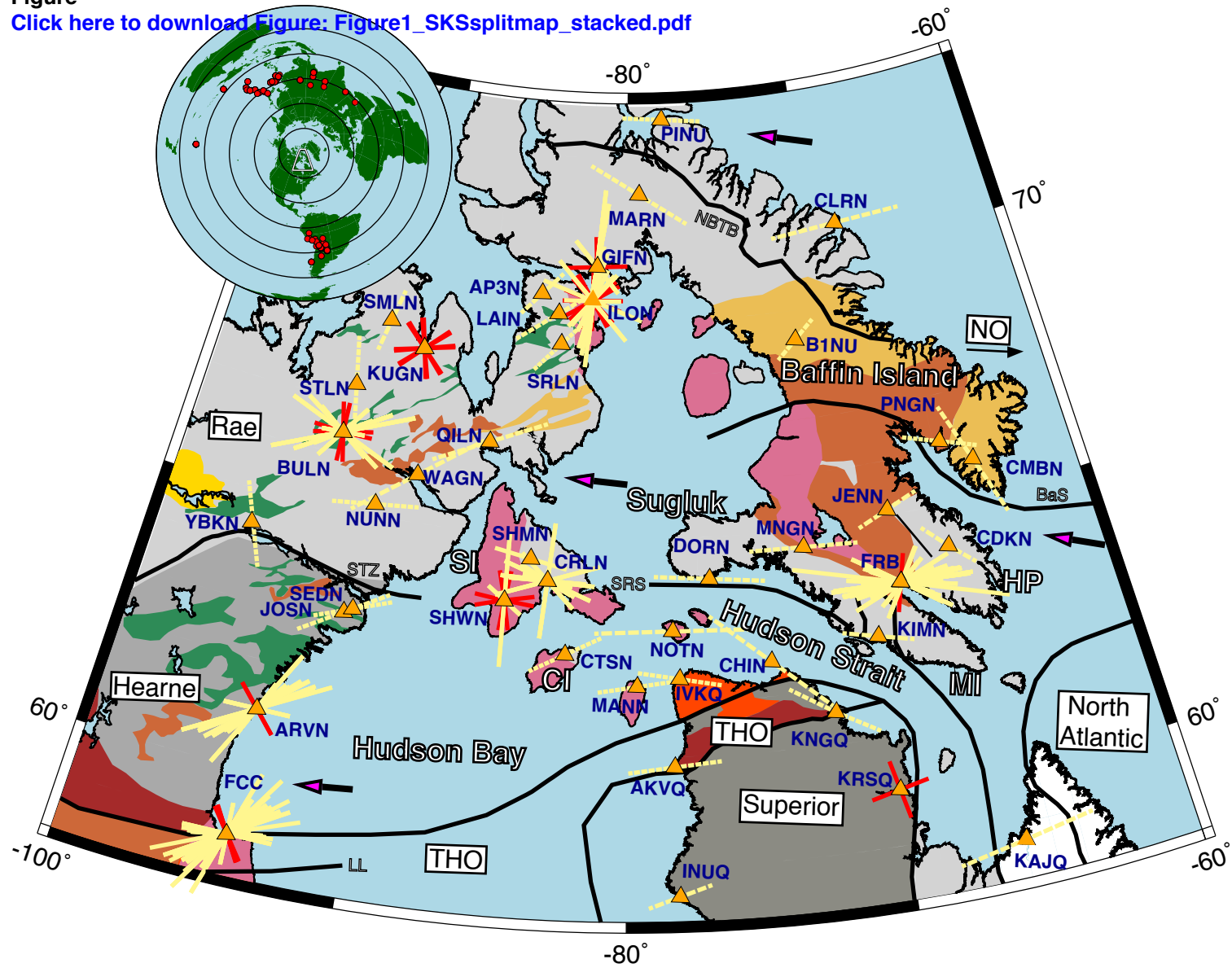
Yuan, H., Romanowicz, B., 2010. Lithospheric layering in the North American craton. Nature 466, 1063–1068.

Yuan, H., Romanowicz, B., Fischer, K. M., Abt, D. L., 2011. 3-D shear wave radially and azimuthally anisotropic velocity model of the North American upper mantle. Geophys. J. Int. 184 (3), 1237–1260.

Zhang, S., Karato, S., I., 1995. Lattice preferred orientation of olivine aggregates deformed in simple shear. Nature 375, 774–777.

Figure

Click here to download Figure: Figure1_SKSsplitmap_stacked.pdf



ARCHEAN

- Rae
- Hearne
- Churchill Plate
- Superior
- Greenstone Terranes

PROTEROZOIC

- Arc Material
- Granite
- Fold Belts
- Sedimentary Rocks
- Baker Lake/Thelon Groups

PHANEROZOIC

- Sedimentary

APM 20 mm/yr

1s

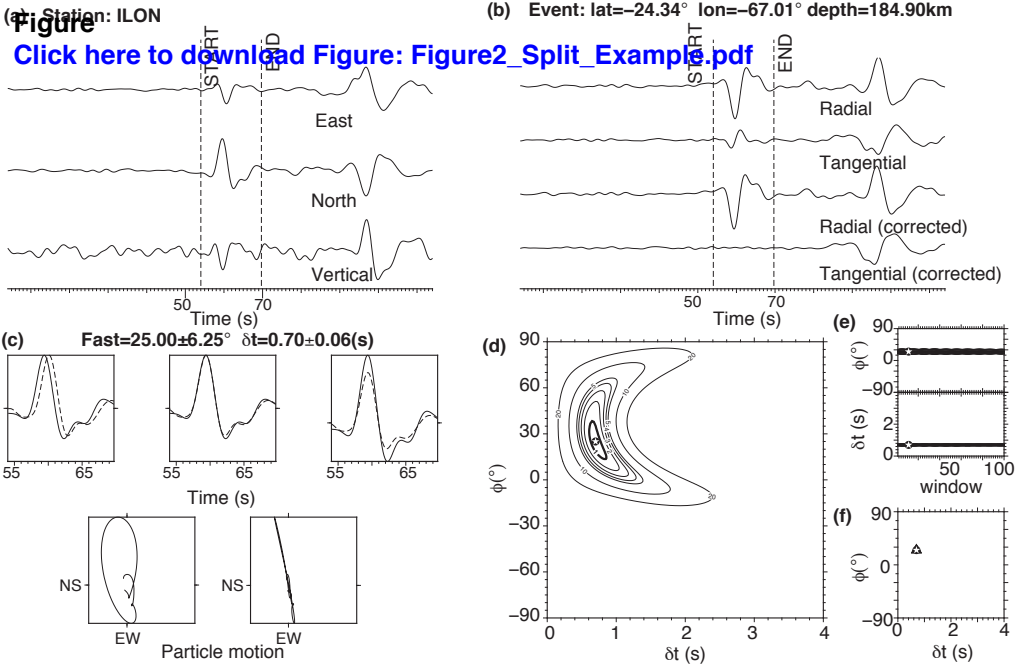
INUQ - Receiver

SRS - Boundary/Region

THO - Craton/Orogen

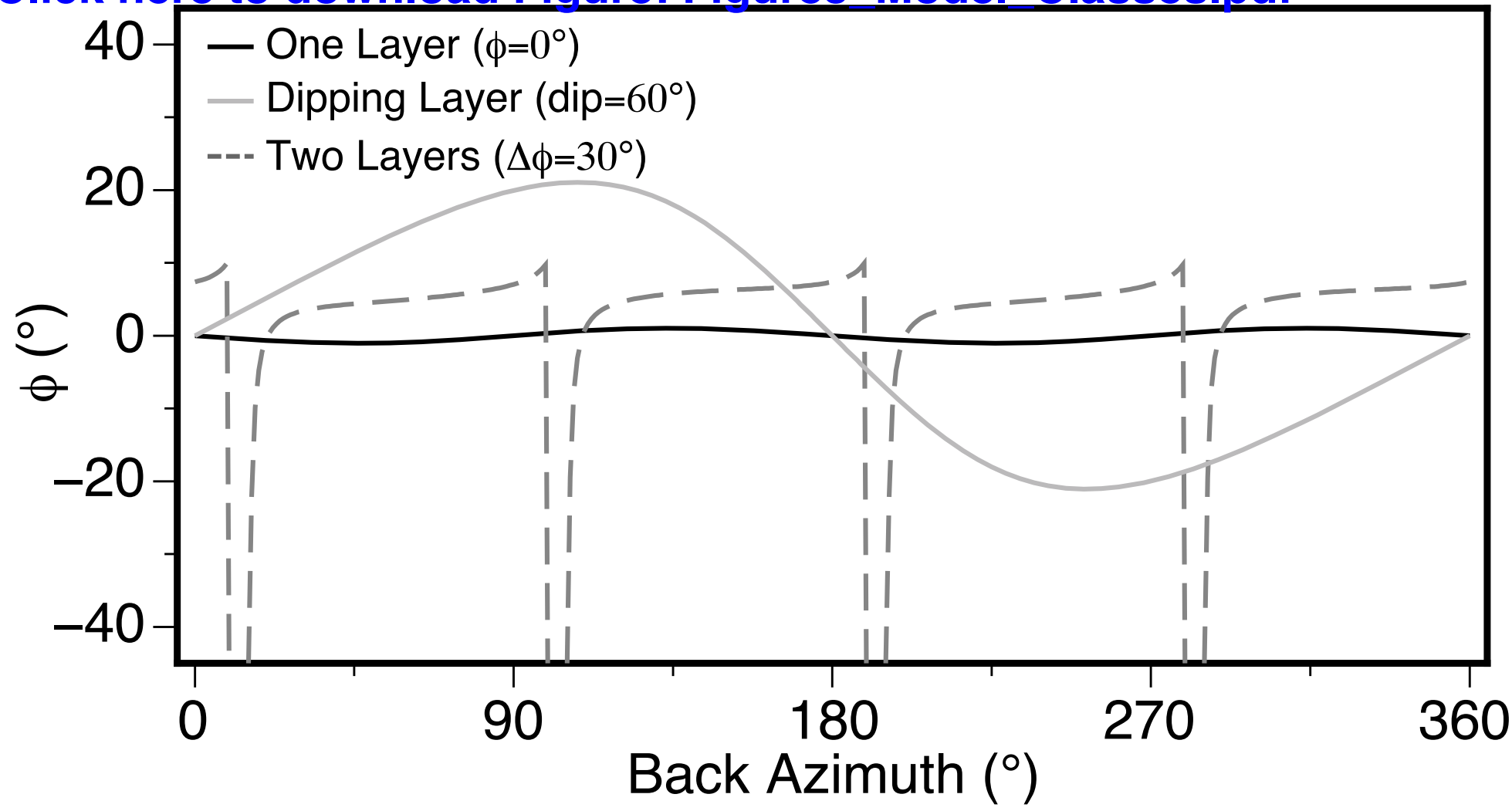
Figure

Click here to download Figure: Figure2_Split_Example.pdf



Figure

Click here to download Figure: Figure3_Model_Classes.pdf



Figure

Click here to download Figure: Figure4_HP_Split_BAZ_colour.pdf

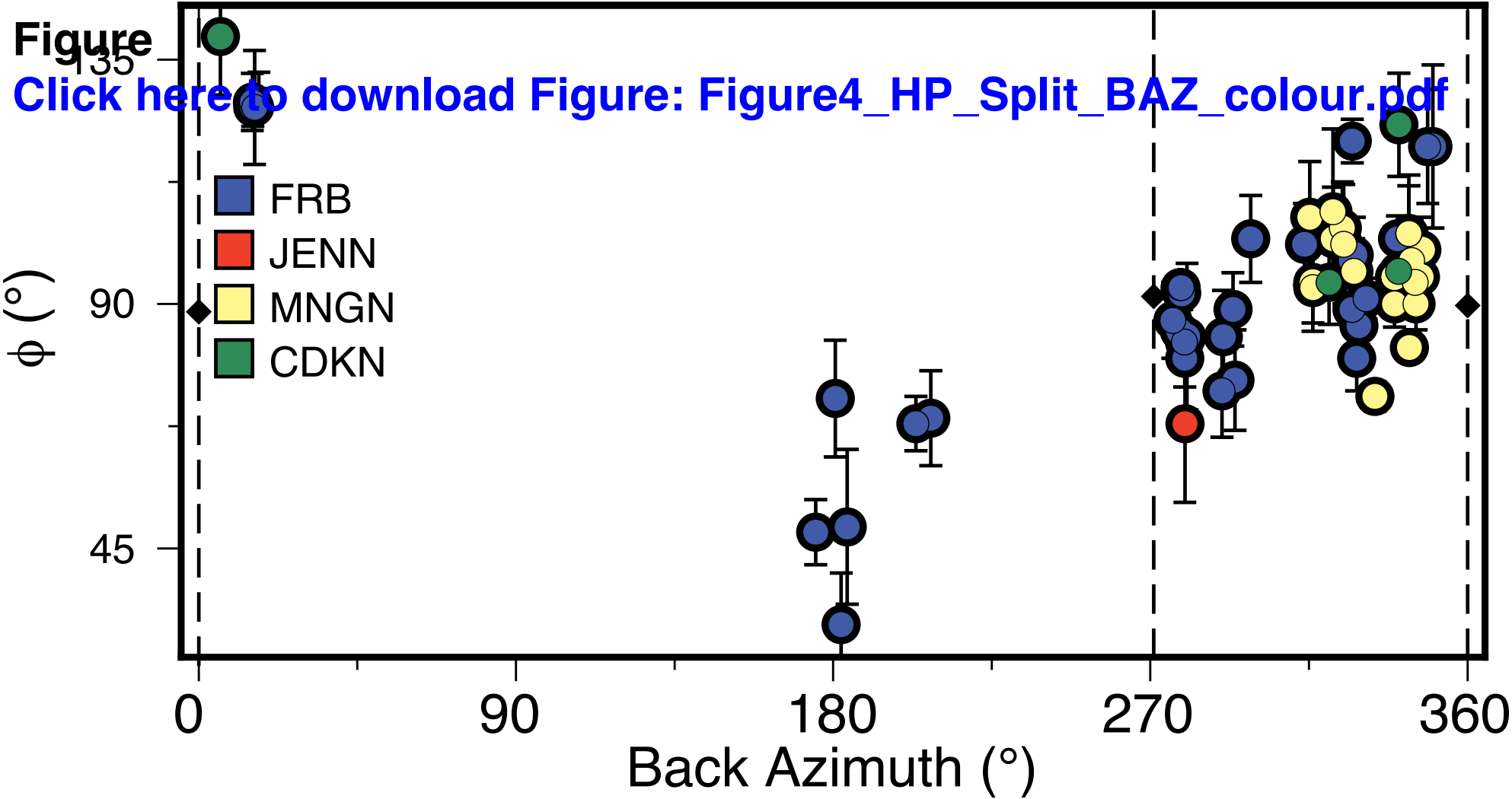
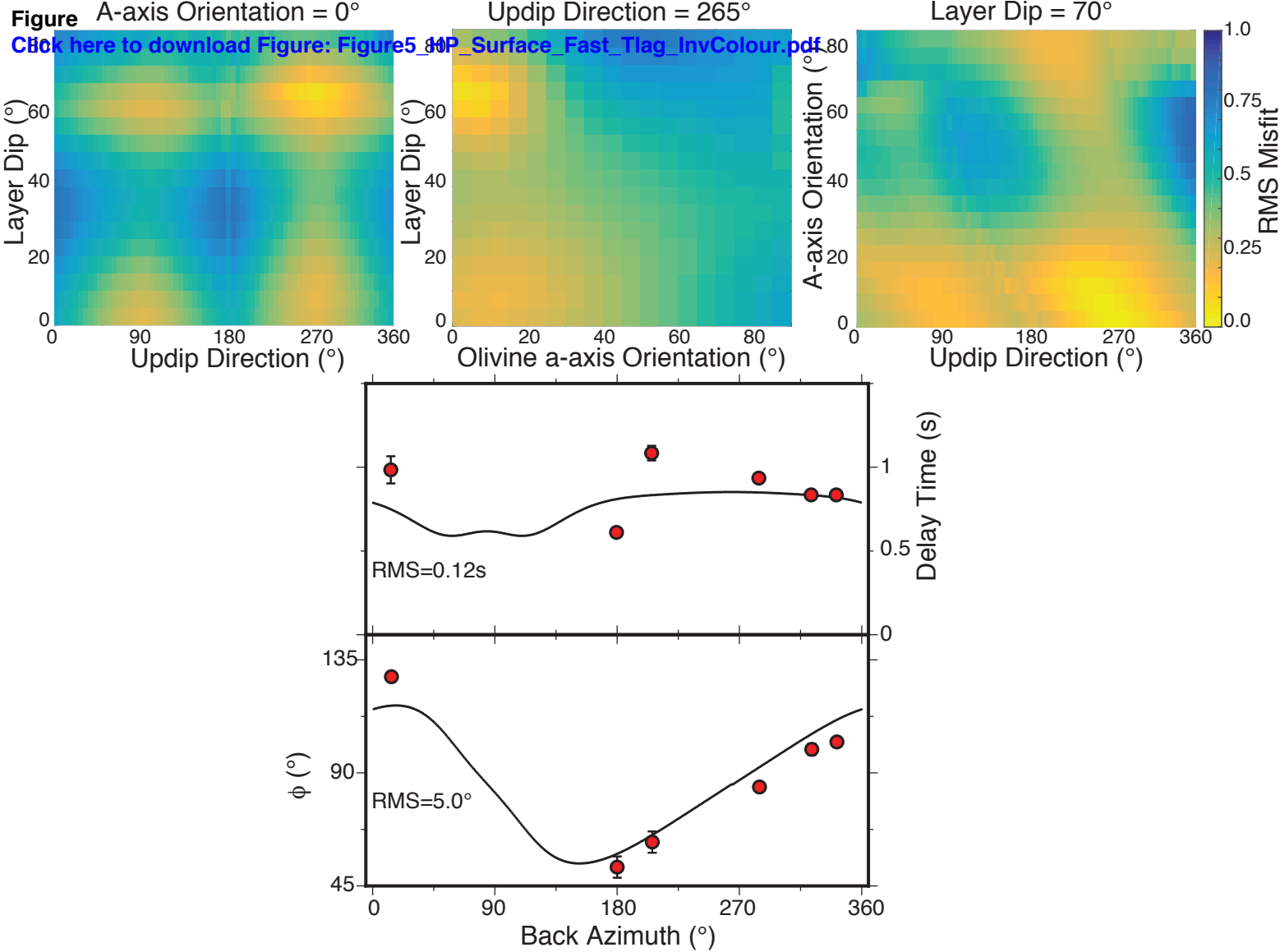
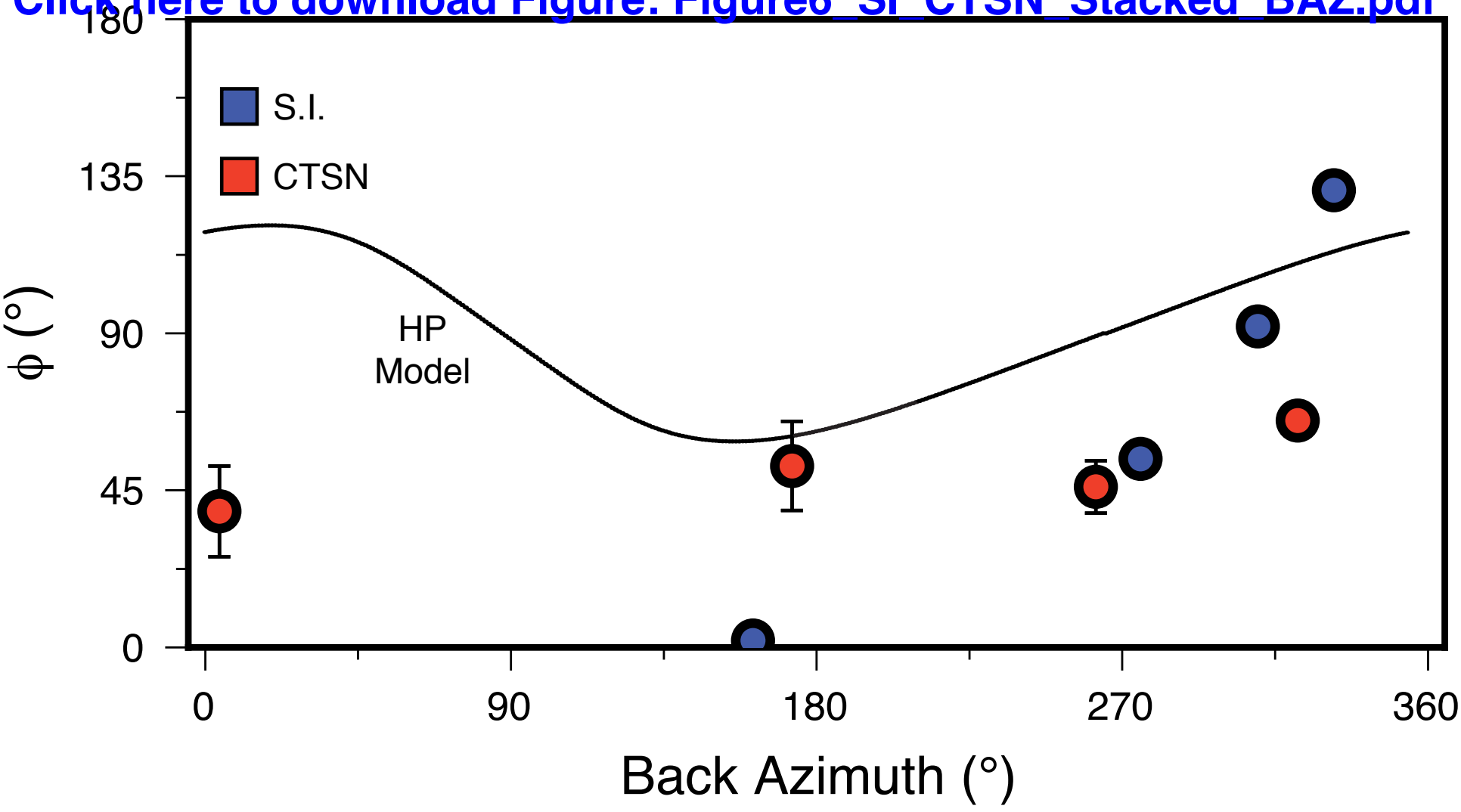


Figure
Click here to download Figure: Figure5_MP_Surface_Fast_Tlag_InvColour.pdf



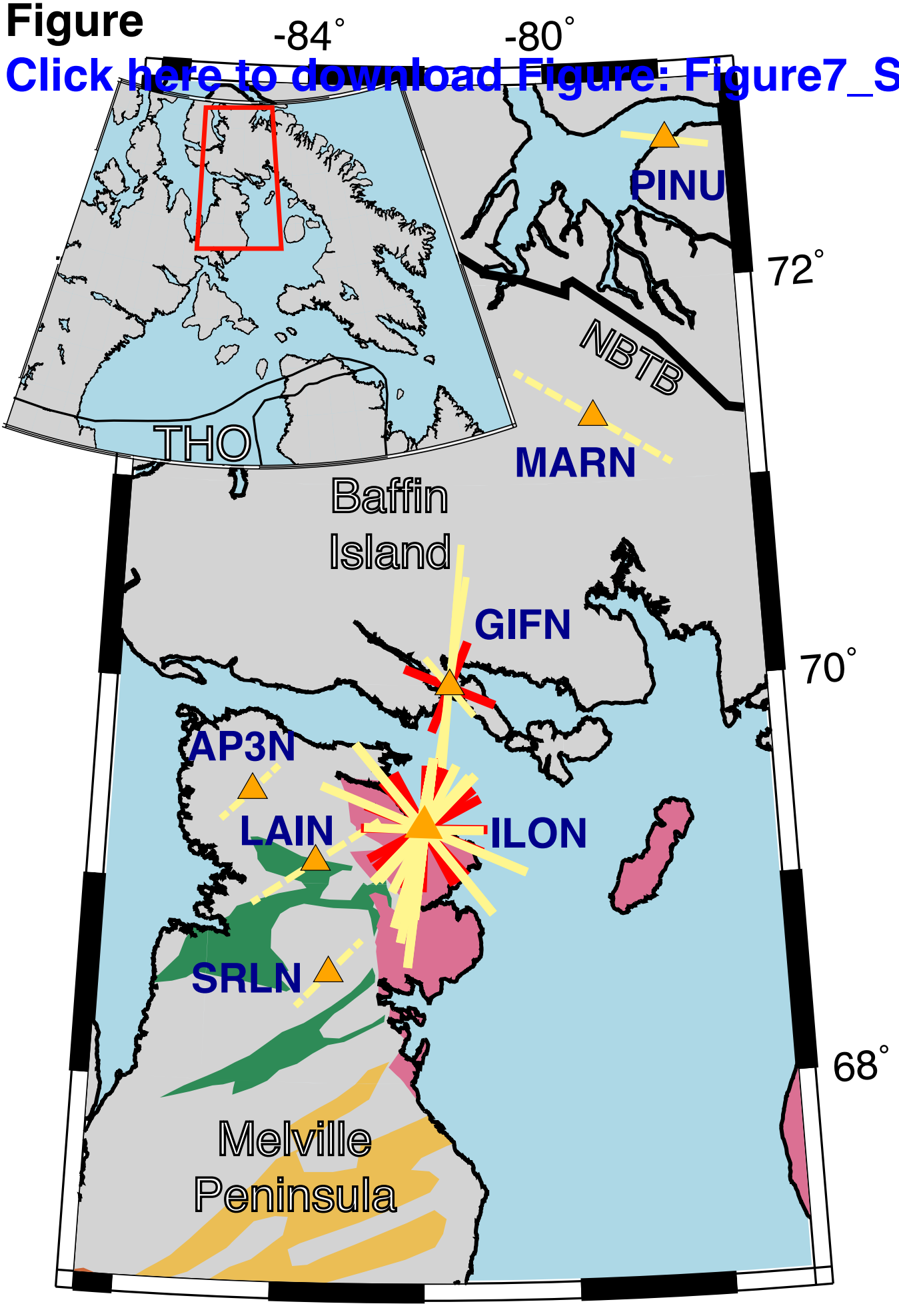
Figure

Click here to download Figure: Figure6_SI_CTSN_Stacked_BAZ.pdf



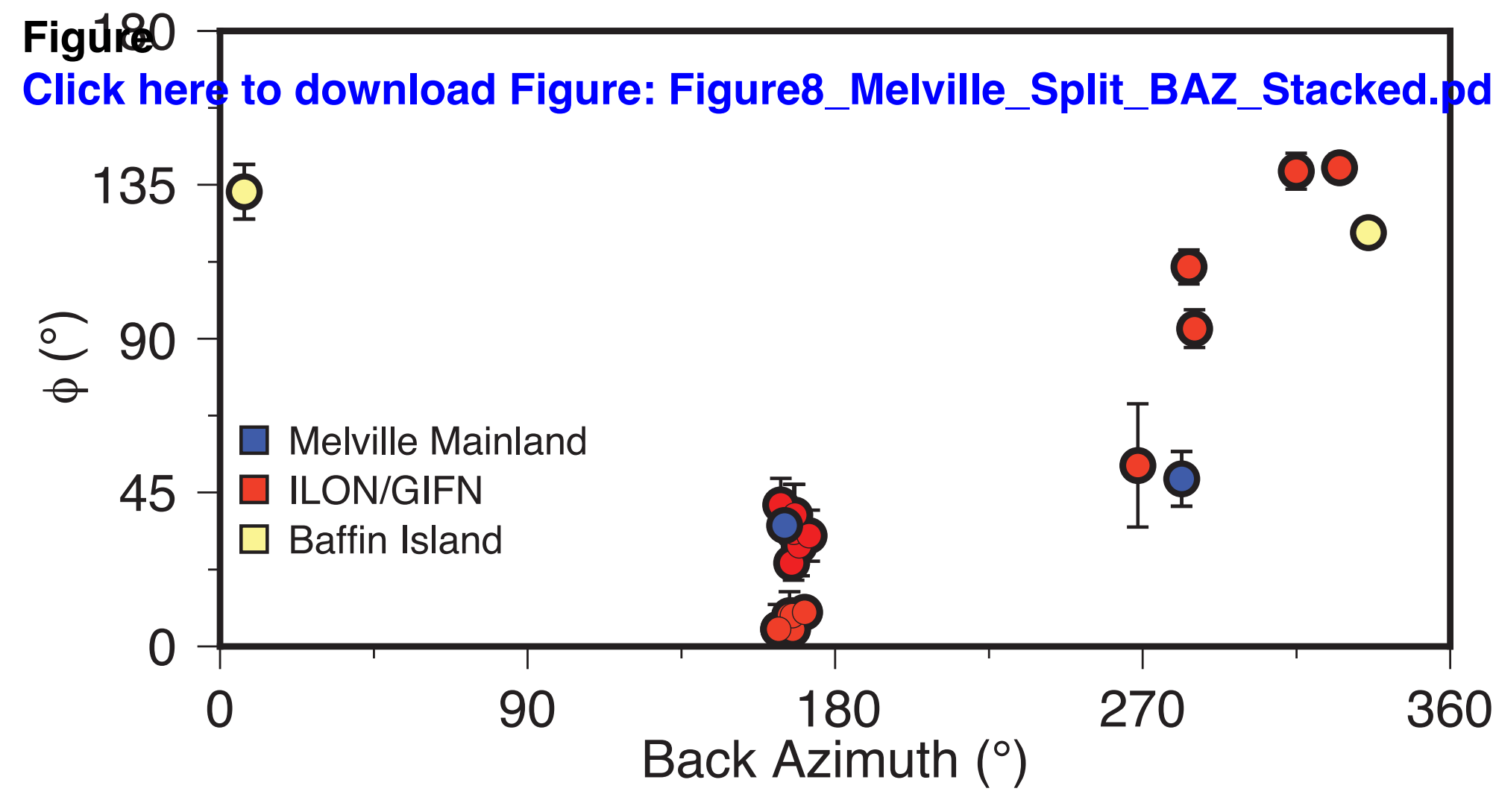
Figure

Click here to download Figure: Figure7_S



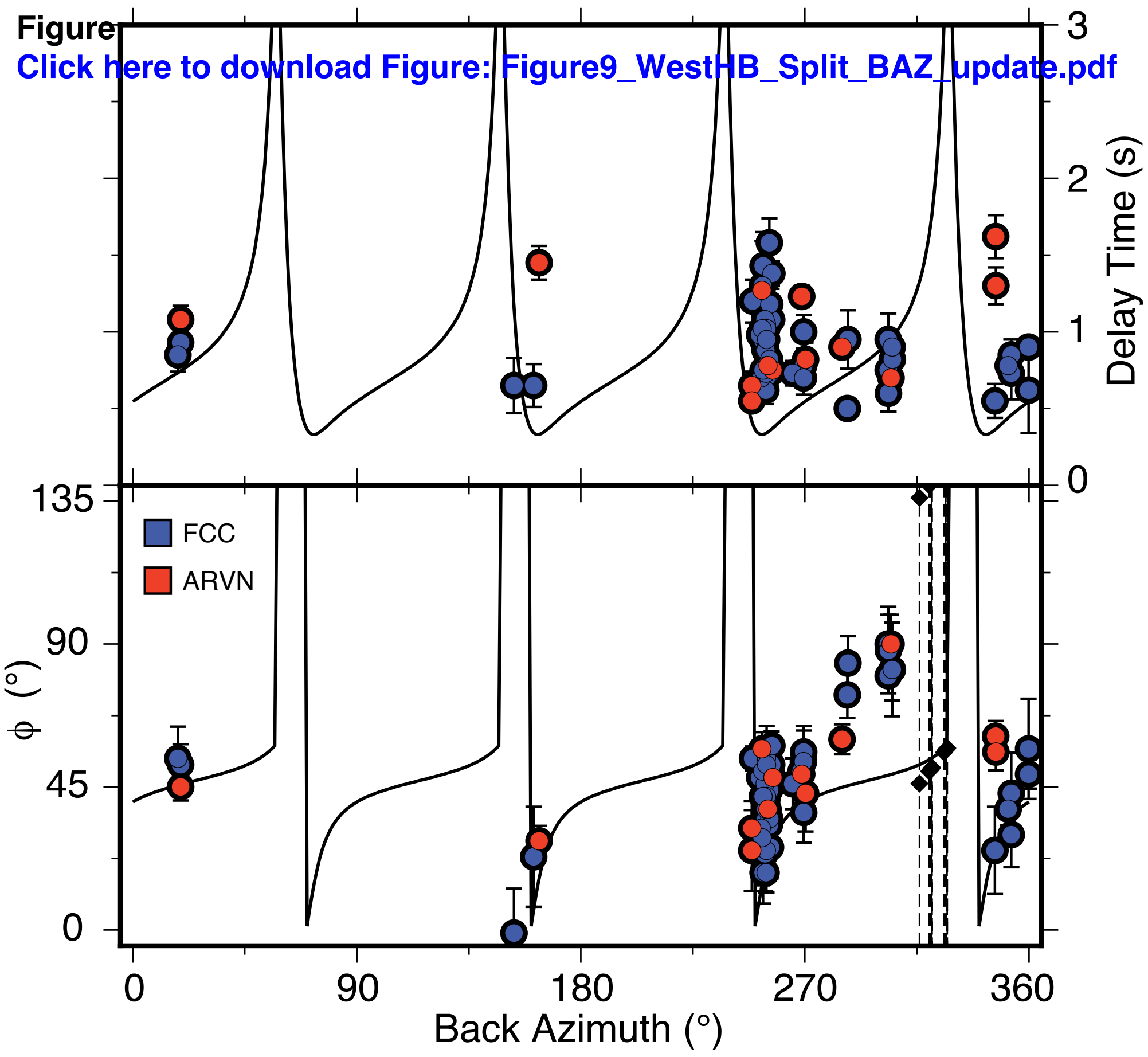
Figure

Click here to download Figure: Figure8_Melville_Split_BAZ_Stacked.pdf



Figure

Click here to download Figure: Figure9_WestHB_Split_BAZ_update.pdf



Supplementary material for online publication only

Click here to download Supplementary material for online publication only: Formation_Laurentia_Supplemental_Reviewed.pdf

LaTeX Source Files

Click here to download LaTeX Source Files: submission_reviewed.tex